





15 **Abstract**

16 Wildfire is an important ecosystem process, influencing land biogeophysical and  
17 biogeochemical dynamics and atmospheric composition. Fire-driven loss of vegetation cover, for  
18 example, directly modifies the surface energy budget as a consequence of changing albedo,  
19 surface roughness, and partitioning of sensible and latent heat fluxes. Carbon dioxide and  
20 methane emitted by fires contribute to a positive atmospheric forcing, whereas emissions of  
21 carbonaceous aerosols may contribute to surface cooling. Process-based modeling of wildfires in  
22 earth system land models is challenging due to limited understanding of human, climate, and  
23 ecosystem controls on fire number, fire size, and burned area. Integration of mechanistic wildfire  
24 models within Earth system models requires careful parameter calibration, which is  
25 computationally expensive and subject to equifinality. To explore alternative approaches, we  
26 present a deep neural network (DNN) scheme that surrogates the process-based wildfire model  
27 within the Energy Exascale Earth System Model (E3SM). The DNN wildfire model accurately  
28 simulates observed burned area with over 90% higher accuracy with a large reduction in  
29 parameterization time compared with the current process-based wildfire model. The surrogate  
30 wildfire model successfully captured global dynamics of wildfire burned area between years  
31 2011 and 2015 ( $R^2 = 0.93$ ). Since the DNN wildfire model has the same input and output  
32 requirements as the E3SM process-based wildfire model, our results demonstrate the  
33 applicability of machine learning for high accuracy and efficient large-scale land model  
34 development and predictions.



## 35 1. Introduction

36 Wildfires burn ~500 million hectares of vegetated land surface each year, which  
37 significantly modifies the physical properties and biogeochemical cycles of terrestrial  
38 ecosystems [Andela *et al.*, 2017; Bond-Lamberty *et al.*, 2007; Pellegrini *et al.*, 2018; Randerson  
39 *et al.*, 2006]. Living vegetation biomass, surface litter, and coarse woody debris are directly  
40 combusted and removed by wildfire [Harden *et al.*, 2006; Walker *et al.*, 2019]. It has been  
41 suggested that global forest would double if fire were eliminated [Bond *et al.*, 2005]. Fire has  
42 multiple important consequences for the climate system, including directly releasing greenhouse  
43 gases (*e.g.*, CO<sub>2</sub>, CH<sub>4</sub>) [Kasischke and Bruhwiler, 2002; Ross *et al.*, 2013] and aerosols [Jiang *et*  
44 *al.*, 2020]; changing land surface albedo and energy budgets [French *et al.*, 2016; Rother and De  
45 Sales, 2020] and land-atmosphere exchanges of heat, mass, and momentum [Chambers and  
46 Chapin, 2002]; limiting plant transpiration and regional water recycling [Brando *et al.*, 2020;  
47 Holden *et al.*, 2018]; and reshaping forest composition [Mekonnen *et al.*, 2019]. In addition,  
48 biomass burning emits a large amount of fine particulate matter that contributes to about 30% of  
49 cloud condensation nuclei globally [Day, 2004]. Soil organic matter decomposition, nitrogen  
50 mineralization, and the richness and diversity of soil fungal communities [Oliver *et al.*, 2015]  
51 could also be influenced by wildfire through modifying litter substrate supply and degraded  
52 enzymatic activities [Bowd *et al.*, 2019; Holden *et al.*, 2018; Pellegrini *et al.*, 2018; Pellegrini *et*  
53 *al.*, 2020].

54 Climate change and land use activities have jointly affected fire spatial distribution,  
55 frequency, and intensity [Andela *et al.*, 2017; Kelley *et al.*, 2019; Xu *et al.*, 2020] since the pre-  
56 industrial era. For example, warmer and drier climate conditions enhance fuel aridity and favor  
57 fire occurrence in forest ecosystems where fuels have built up over a period of decades and  
58 centuries [Abatzoglou and Williams, 2016; Williams *et al.*, 2019]. Even if annual precipitation  
59 does not decline, redistribution of precipitation towards wet season extreme rainfall events could  
60 contribute to longer dry periods and thus more severe fire activity [Xu *et al.*, 2020]. Human  
61 activities often shape wildfire activity through regulating patterns of ignition and fire occurrence  
62 (*e.g.*, powerline ignition) [Keeley and Syphard, 2018] and suppressing wildfire activity by means  
63 of land fragmentation, fire management, and livestock grazing [Andela *et al.*, 2017]. In  
64 California, fire density is highly associated with population density and the distance to the  
65 wildland urban interface (WUI) [Syphard *et al.*, 2007]. At the global scale, along gradients of



66 increasing population density, fire frequency initially increases by up to 20% and then gradually  
67 declines in more densely populated areas [Knorr *et al.*, 2014].

68 Although global wildfire burned area has declined over the recent two decades [Andela *et*  
69 *al.*, 2017], many vulnerable ecosystems and geographic regions have experienced significant  
70 increases in wildfire activity [Abatzoglou and Williams, 2016; Walker *et al.*, 2019] resulting in  
71 large losses of natural resources and economic assets [Papakosta *et al.*, 2017; Stephenson *et al.*,  
72 2013]. Over western U.S. forests, wildfire has dramatically increased, costing billions of dollars  
73 each year and gaining wide public attention. This regional wildfire increase is mainly driven by  
74 concurrent increases of spring temperature and declining snowpack [Westerling *et al.*, 2006],  
75 mid-summer increases in vapor pressure deficit [Williams *et al.*, 2019], and increases in drought  
76 stress during fall [Goss *et al.*, 2020]. The enhancement of wet and dry oscillations favors initial  
77 vegetation growth and subsequent wildfire activity [Heyerdahl *et al.*, 2002; Saha *et al.*, 2019].

78 Wildfire models have played an important role in many aspects of wildfire research,  
79 including monitoring fire spread [Finney, 1998; Radke *et al.*, 2019], analyzing controllers of  
80 wildfire short-term and long-term variability [Kelley *et al.*, 2019], predicting severity of the  
81 upcoming fire seasons [Preisler and Westerling, 2007] and climate-scale fire variability  
82 [Girardin and Mudelsee, 2008; Yue *et al.*, 2013], and understanding the complex climate-  
83 wildfire-ecosystem feedbacks [Clark *et al.*, 2004; Mekonnen *et al.*, 2019; Zou *et al.*, 2020]. Two  
84 types of wildfire models are widely used: process-based models and data-driven statistical  
85 models. Process-based wildfire models consider detail processes related to natural fire ignition  
86 [Prentice and Mackerras, 1977], anthropogenic ignition [Venevsky *et al.*, 2002], fire spread and  
87 duration [Thonicke *et al.*, 2010], fire suppression [Lenihan and Bachelet, 2015], and fire mass  
88 and heat fluxes [Li *et al.*, 2012]. Process-based wildfire models have been widely used in  
89 dynamic vegetation models and coupled earth system models (ESMs) with various complexities  
90 of parameterization [Li *et al.*, 2019]. As more and more detailed fire processes are considered  
91 and parameterized, structural and parametric uncertainties may increase due to incomplete  
92 representation of individual processes and imperfect mathematical formulation [Riley and  
93 Thompson, 2017].

94 Although explicit processes are simulated, the accuracy of process-based wildfire models  
95 are highly dependent on parameterization, which is computationally expensive [Teckentrup *et*  
96 *al.*, 2018; Zhu and Zhuang, 2014]. Data-driven models, however, directly link the driving



97 variables (*e.g.*, climate factors) to the fire activity using simple statistical models or more  
98 sophisticated machine learning techniques, ignoring the explicit processes and feedbacks  
99 associated with wildfire [*Ganapathi Subramanian and Crowley, 2018; Radke et al., 2019; Tonini*  
100 *et al., 2020*]. Through training and validation, statistical representations of wildfire dynamics are  
101 learned by models using principles from machine learning. Data-driven wildfire models are  
102 diverse in terms of driving variables and model structure. For example, many current machine  
103 learning wildfire models rely on remote oceanic dynamics (*e.g.*, sea surface temperature  
104 variability) and atmospheric teleconnections to simulate land surface fire activities [*Chen et al.,*  
105 *2020; Chen et al., 2011; Yu et al., 2020*]. Another group of data-driven wildfire models draws  
106 more heavily upon regional climate, plant functional type, and human infrastructure driver  
107 variables [*Coffield et al., 2019; Sayad et al., 2019*].

108 In this study, we develop a machine learning wildfire model using the process  
109 representation of wildfire in the Energy Exascale Earth System Model (E3SM) land model  
110 (ELMv1) [*Zhu et al., 2019*] the observationally-inferred Global Fire Emissions Database v4  
111 (GFEDv4), and a deep neural network approach [*Goodfellow et al., 2016*]. We implemented a  
112 deep learning model that can better capture the complex and non-linear interactions between  
113 controlling factors and wildfire activity. The objectives of this study are to surrogate the wildfire  
114 parameterization in ELMv1 with the deep neural network and improve the model simulated  
115 wildfire burned area across various fire regions [*Giglio et al., 2013*].

116

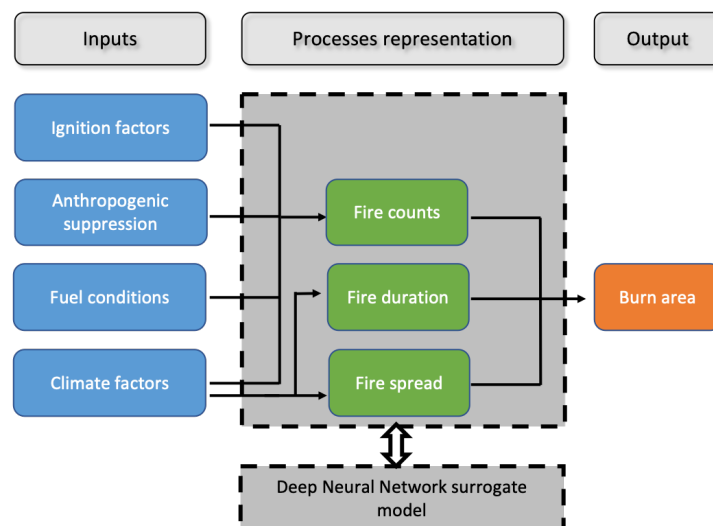
## 117 **2. Methodology**

### 118 **2.1 ELMv1 wildfire model**

119 The process-based wildfire model in ELMv1 originates from the Community Land  
120 Model (CLM4.5) [*Li et al., 2012*]; we take this wildfire model as the baseline (hereafter refer to  
121 as BASE-Fire). BASE-Fire combines information regarding ignition, fuel conditions, surface  
122 climate, and anthropogenic suppression to simulate total burned area based on the fire counts and  
123 spread area of each fire (Figure 1). The fire count in BASE-Fire is modeled as the sum of  
124 anthropogenic ignition and natural ignition, where the latter is proportional to lightning density  
125 [*Prentice and Mackerras, 1977*] and the former is determined by population density [*Venevsky et*  
126 *al., 2002*]. Human activity may also intentionally suppress wildfire occurrence if the fire is  
127 detected at early stage. For example, developed regions with high population density and gross



128 domestic product are less likely to use fire to remove surface biomass. On the other hand,  
129 developed regions more likely suppress fire given more effective fire management policy and  
130 suppression capability. Fire count is also affected by surface fuel availability (aboveground  
131 biomass) and fuel combustibility (relative humidity, topsoil temperature and moisture). The fire  
132 spread area in BASE-Fire is modeled as an elliptical shaped region controlled by wind speed and  
133 fuel wetness (using topsoil (0 – 15 cm) moisture as a proxy). The fire duration is set to be one  
134 day based on a study that reported years 2001-2004 mean global fire persistence [Giglio *et al.*,  
135 2006a]. BASE-Fire also does not explicitly consider roads, rivers, and firefighting activity  
136 [Arora and Boer, 2005].  
137



138  
139 **Figure 1.** Schematic representation of the ELMv1 process-based BASE-Fire model and the  
140 components to be surrogated with the Deep Neural Network (DNN) model (dark grey).

141  
142 **2.2 Deep neural network wildfire surrogate model**

143 We developed the new fire model in two steps: (1) surrogating BASE-Fire with a deep  
144 neural network (DNN) approach and (2) improving that surrogate model using the Global Fire  
145 Emissions Database v4 (GFEDv4 [Giglio *et al.*, 2013]). First, we surrogated BASE-Fire with a  
146 DNN approach (hereafter refer to as DNN-Fire) that uses the same input and output variables as  
147 BASE-Fire but treats the explicit intermediate processes (*e.g.*, ignition, fire spread) as latent  
148 variables coded by hidden layers in the DNN (Figure 1). DNN-Fire was developed with five



149 hidden layers and five neurons in each layer for burned area simulation. The DNN approach uses  
 150 a fully-connected feedforward neural network [Schmidhuber, 2015] that comprises input, hidden,  
 151 and output layers:

$$h_1 = f_1(W_1 I + b_1) \quad (1)$$

$$h_2 = f_2(W_2 h_1 + b_2) \quad (2)$$

$$h_3 = f_3(W_3 h_2 + b_3) \quad (3)$$

$$h_4 = f_4(W_4 h_3 + b_4) \quad (4)$$

$$h_5 = f_5(W_5 h_4 + b_5) \quad (5)$$

$$O = f_6(W_6 h_5 + b_6) \quad (6)$$

152 where  $I$  denotes the input layer (*e.g.*, climate factors) with 11 neurons, each corresponding to an  
 153 input variable listed in Table 1.  $h_1$ ,  $h_2$ ,  $h_3$ ,  $h_4$ , and  $h_5$  are five hidden vectors that are calculated  
 154 with two steps. First is a linear combination of previous layers' input vector ( $h$ ) and the trainable  
 155 weight parameter matrix [ $W_1$ ,  $W_2$ ,  $W_3$ ,  $W_4$ ,  $W_5$ ,  $W_6$ ], considering biases  $b_1$ ,  $b_2$ ,  $b_3$ ,  $b_4$ ,  $b_5$ , and  $b_6$ .  
 156 Then, nonlinear activation functions  $f_1$ ,  $f_2$ ,  $f_3$ ,  $f_4$ ,  $f_5$ , and  $f_6$  are applied to the output from the  
 157 previous step. In this study we used *softplus* as the activation function [Zheng *et al.*, 2015] that is  
 158 a non-linear transformation of input signals.  $O$  denotes the output layer that summarize the latent  
 159 variables from the last hidden layer ( $h_5$ ) and calculate burned area.

160

161 **Table 1.** Input and output variables of ELMv1 BASE-Fire and surrogate DNN-Fire models

Variable category	Variable name	Data source	Reference
<i>Input variables</i>			
	Tree coverage	LUH2	[Hurt et al., 2020]
	Fuel load	ELMv1 total biomass	[Zhu and Riley, 2015; Zhu et al., 2019]
<b>Fuel conditions</b>	Fuel wetness	ELMv1 topsoil moisture	[Zhu and Riley, 2015; Zhu et al., 2019]
	Fuel temperature	ELMv1 topsoil temperature	[Zhu and Riley, 2015; Zhu et al., 2019]
<b>Climate factors</b>	Precipitation	GSWP3	[Dirmeyer et al., 2006]



	Near surface temperature	GSWP3	[Dirmeyer et al., 2006]
	Wind speed	GSWP3	[Dirmeyer et al., 2006]
	Relative humidity	GSWP3	[Dirmeyer et al., 2006]
<b>Ignition</b>	Population density	-	[Dobson et al., 2000]
	Lightning frequency	NASA-LIS/OTD	[Cecil et al., 2014]
<b>Anthropogenic suppression</b>	GDP	-	[van Vuuren et al., 2007]
	Population density	-	[Dobson et al., 2000]
<i>Output variable</i>			
	Burned area	ELMv1 percentage burned area	[Zhu and Riley, 2015; Zhu et al., 2019]

162

163 Second, we improved the surrogate DNN-Fire by fine-tuning the weight parameters using  
 164 observations (hereafter refer to DNN-Fire-GFED). Between 2001 and 2010, we initialized  
 165 DNN-Fire-GFED's weight parameters ( $W_1$ ,  $W_2$ ,  $W_3$ ,  $W_4$ ,  $W_5$ , and  $W_6$ ) using results from DNN-  
 166 Fire, replaced the BASE-Fire burned area by GFEDv4 burned area [Giglio et al., 2013], and  
 167 adjusted weight parameters until the model best reproduced the observed burned area. This two-  
 168 step approach will also allow rapid parameterization of the Fire model as new fire data and  
 169 baseline fire model results become available. DNN-Fire-GFED can be more easily generalized  
 170 since BASE-Fire provides explicit physical guidance and a larger-than-observation input and  
 171 output feature space for development of the machine learning fire model.

### 172 **2.3 Model setup and simulation protocol**

173 We ran ELMv1 with BASE-Fire at 1.9° by 2.5° spatial resolution [Zhu et al., 2020; Zhu  
 174 et al., 2016] to generate training and testing datasets for the DNN wildfire model. BASE-Fire  
 175 was first spun up for 600 years with accelerated soil decomposition followed by 200 years  
 176 regular spinup with regular soil decomposition [Koven et al., 2013]. The spinup simulations were  
 177 forced with constant atmospheric CO<sub>2</sub> concentration (285 ppmv) and 1901-1920 repeated  
 178 climate forcing from GSWP3 (Global Soil Wetness Project) [Dirmeyer et al., 2006]. The purpose  
 179 of the spinup was to initialize ecosystem carbon pools and stabilize plant and soil carbon and  
 180 water fluxes. Restarting from the spinup conditions, a transient simulation was then conducted  
 181 from 1901 to 2015 with GSWP3 transient climate forcing, atmospheric CO<sub>2</sub> concentrations, and



182 nitrogen and phosphorus deposition [Lamarque et al., 2005; Mahowald et al., 2008]. Wildfire  
183 associated variables were selected for output with a monthly temporal resolution (Table 1).

184 BASE-Fire output from years 1981 to 2010 were used to train, test, and fine-tune  
185 DNN-Fire. We developed 14 region-specific models, corresponding to 14 widely used GFEDv4  
186 regions. For each region, all GFEDv4 land gridcells (comprising no fire history, infrequent fire,  
187 and repeated fire) were concatenated into one data matrix (where rows consist of the number of  
188 samples and columns of the number of variables). 80% of the data matrix was randomly sampled  
189 for the training dataset and the remaining 20% of the data were reserved for testing. All training  
190 and testing datasets were normalized to the range [0, 1] with the following scaler:

$$X = \frac{X - X_{min}}{X_{max} - X_{min}} \quad (7)$$

191 where  $X$  is the variable vector of interest and  $X_{min}$  and  $X_{max}$  are minimum and maximum values of  
192  $X$ , respectively. During the training stage, we randomly initialized the weighting parameters (Eq.  
193 1-6) and optimized them using the Adaptive Moment Estimation method [Kingma and Ba,  
194 2014], which is a variant of the gradient descent optimization method but considers adaptive  
195 learning rate and momentum-like exponentially decaying gradients. The parameter optimization  
196 aimed to minimize a mean squared error cost function:

$$J = \frac{1}{n} \sum_{i=1}^n (y_i^{DNN} - y_i^{BASE})^2 \quad (8)$$

197 where  $y_i^{DNN}$  and  $y_i^{BASE}$  are DNN-Fire and BASE-Fire generated burned area, respectively. Cost  
198 function  $J$  summarizes the overall magnitude of the error between the surrogate DNN-Fire and  
199 BASE-Fire. We then evaluated model performance using metrics of mean absolute error

200  $(\frac{1}{n} \sum_{i=1}^n |y_i^{DNN} - y_i^{BASE}|)$ , Pearson correlation  $(\frac{covariance(y^{DNN}, y^{BASE})}{\sqrt{variance(y^{DNN})variance(y^{BASE})}})$ , and coefficient of

201 determination  $(R^2 = 1 - \frac{\sum_{i=1}^n (y_i^{DNN} - y_i^{BASE})^2}{\sum_{i=1}^n (y_i^{BASE} - y_{mean}^{BASE})^2})$ .

202

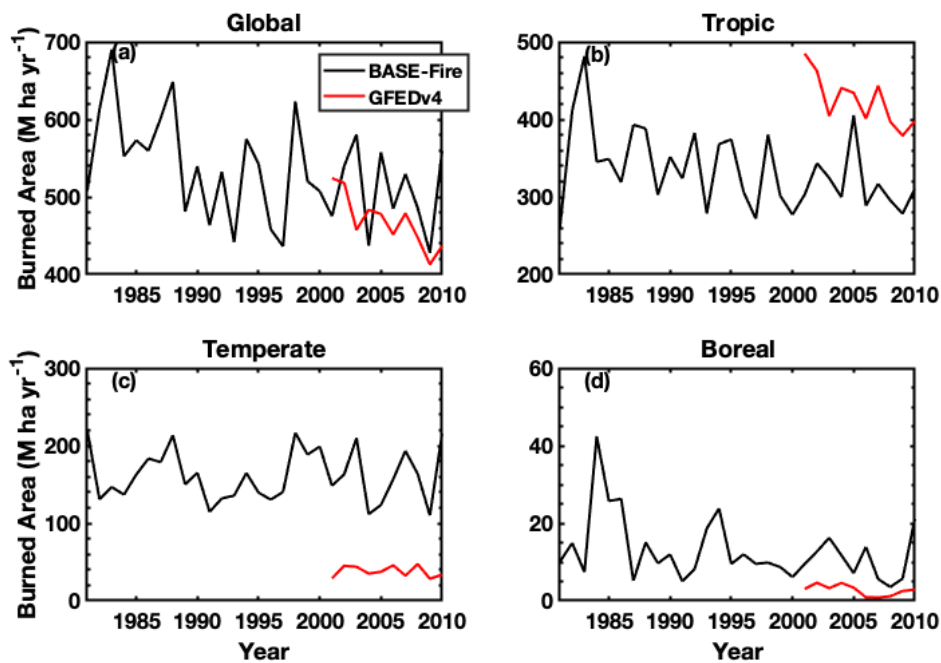
### 203 3. Results and discussion

#### 204 3.1 Evaluation of wildfire surrogate model

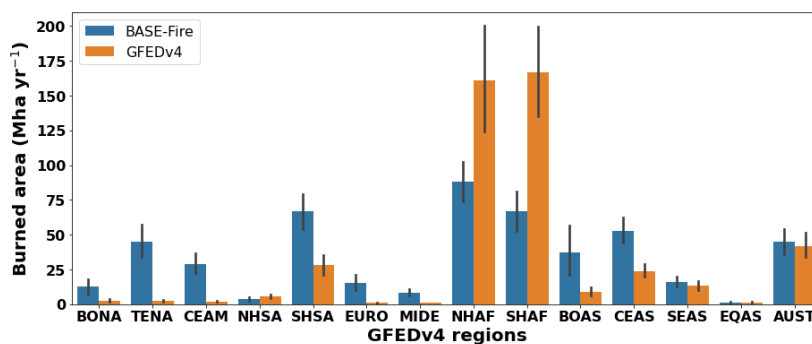
205 BASE-Fire performed reasonably well for total global burned area ( $508 \pm 53$  Mha yr<sup>-1</sup>  
206 (million hector per year) between years 2001 and 2010 compared with the GFEDv4 value of  $469$   
207  $\pm 35$  Mha yr<sup>-1</sup>; Figure 2). BASE-Fire also captured the global declining trend of wildfire burned  
208 area over this time period, attributed to a decrease in tropical fires [Andela et al., 2017]. At the



209 regional scale, however, BASE-Fire underestimated tropical (S23.5° - N23.5°) burned area and  
210 overestimated temperate (N23.5° - N67.5°) and boreal (N67.5 above) burned area (Figure 2).  
211 Large spatial heterogeneity existed for BASE-Fire regional bias. For example, over tropical  
212 GFEDv4 regions, BASE-Fire overestimated wildfire burned area over Southern Hemisphere  
213 South America (SHSA), but underestimated wildfire burned area over both Southern and  
214 Northern Hemisphere Africa regions (SHAF and NHAF), despite an overall underestimation  
215 over the tropical region (Figure 3). In contrast, consistent overestimation occurred over all  
216 temperate GFEDv4 regions. For example, wildfire burned was overestimated by about a factor of  
217 16 (~1 versus 16 Mha yr<sup>-1</sup>) over the Europe GFEDv4 region (EURO) (Figure 3). Although there  
218 is room to improve BASE-Fire performance, the parameterization would involve large ensemble  
219 simulations and computational resources. Instead, we first use BASE-Fire generated data as  
220 training and validation datasets to parameterize DNN-Fire against observed burned area.



221  
222 **Figure 2.** BASE-Fire simulated and GFEDv4 observationally inferred burned area at (a) global  
223 scale; (b) Tropical (S23.5° -N23.5°); (c) Temperate (N23.5° - N 67.5°); and (d) Boreal (north of  
224 N 67.5°) regions.



225

226 **Figure 3.** A comparison of wildfire burned area between estimates from the ELMv1 process-  
227 based model (BASE-Fire) and GFEDv4 observations over 14 regions.

228

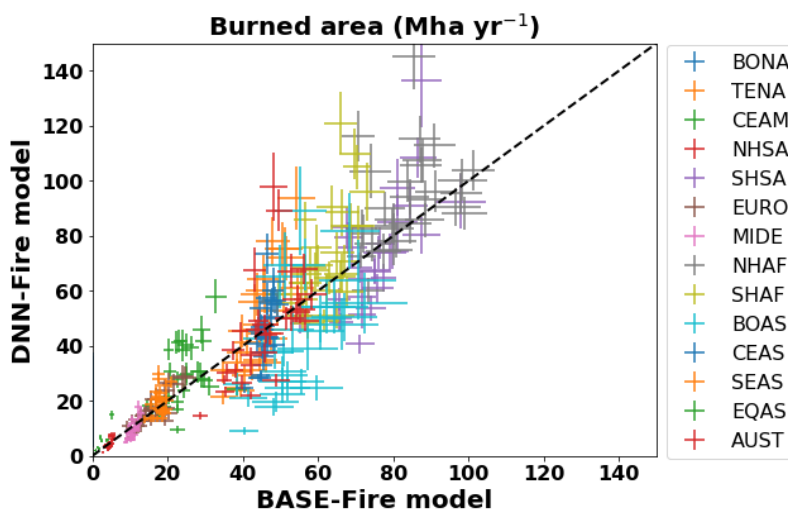
229 Next we compare DNN-Fire and BASE-Fire outputs of burned area. Using BASE-Fire  
230 generated  $1.9^\circ \times 2.5^\circ$  resolution datasets of surface fuel conditions (fuel load (vegetation  
231 biomass), fuel temperature (topsoil temperature), and fuel wetness (topsoil moisture)) with  
232 gridded climate forcing (GSWP3) [Dirmeyer et al., 2006], land use (LUH2 dataset) [Hurt et al.,  
233 2020], and social economic [Dobson et al., 2000; van Vuuren et al., 2007] factors, DNN-Fire  
234 captured the spatial pattern of BASE-fire predicted wildfire activity (Figure 4). Across all  
235 GFEDv4 regions, mean absolute error of DNN-Fire was  $4.4 \text{ Mha yr}^{-1}$  ( $<1\%$  of total burn area),  
236 with median and maximum errors of  $1.8$  and  $13.0 \text{ Mha yr}^{-1}$ , respectively (Figure 5). Equatorial  
237 Asia (EQAS), Northern Hemisphere South America (NHSA), Central America (CEAS), and  
238 Europe (EURO) regions had the lowest DNN-Fire errors ( $< 1.0 \text{ Mha yr}^{-1}$ ), while Southern  
239 Hemisphere Africa (SHAF), and Boreal Asia (BOAS) had the largest errors ( $10\text{-}13 \text{ Mha yr}^{-1}$ ).  
240 Overall, the correlation coefficient between BASE-Fire and DNN-Fire simulated burned area  
241 was  $0.91$  ( $p$  value  $< 0.01$ ) and the coefficient of determination ( $R^2$ ) was  $0.79$ . Across seasons,  
242 DNN-Fire also reasonably captured the BASE-Fire peak fire months (June to October), which  
243 were dominated by Southern Hemisphere Africa and Southern Hemisphere South America  
244 (Figure 6, orange and blue lines).

245

246 By surrogating BASE-Fire, DNN-Fire is expected to have similar biases and  
247 uncertainties. The deficiency of BASE-Fire model will propagate to DNN-Fire. In our future  
248 work we will overcome such limitation by training multiple DNN-Fire models with ensemble  
simulations of BASE-Fire models that differ in critical parameters and vary in model structures.



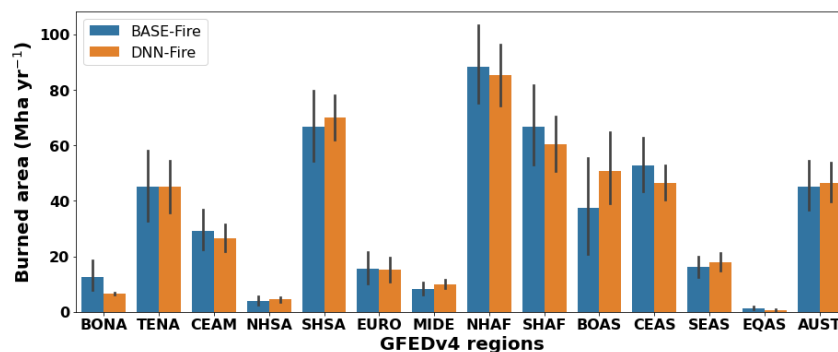
249



250

251 **Figure 4.** The performance of the Deep Neural Network wildfire model (DNN-Fire), compared  
 252 with the original ELMv1 process-based wildfire model (BASE-Fire) over 14 GFEDv4 regions  
 253 between years 2001 and 2010.

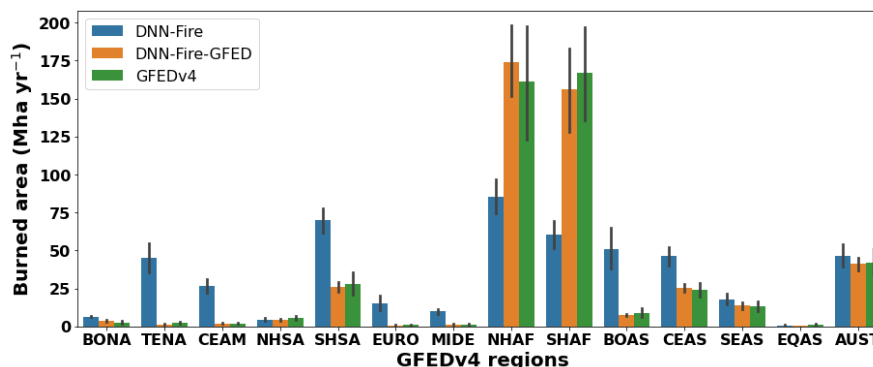
254



255

256 **Figure 5.** A comparison of wildfire burned area between the original ELMv1 process-based  
 257 wildfire model (BASE-Fire) and Deep Neural Network wildfire model (DNN-Fire) over 14  
 258 GFEDv4 regions. Error bars represent temporal (2001-2010) standard deviation for each  
 259 GFEDv4 region.

260



261

262 **Figure 6.** A comparison of wildfire burned area among Deep Neural Network wildfire model  
263 (DNN-Fire), Deep Neural Network wildfire model fine-tuned with GFEDv4 (DNN-Fire-GFED),  
264 and observations over 14 GFEDv4 regions. Error bars represent temporal (2001-2010) standard  
265 deviation for each GFEDv4 region.

266

### 267 3.2 Calibrating the wildfire surrogate model using GFEDv4

268 Although the global pattern was reasonably captured, BASE-Fire had relatively large  
269 biases in several GFEDv4 regions, as discussed above. Since DNN-Fire was trained and  
270 validated only with BASE-Fire generated inputs (*e.g.*, fuel conditions) and outputs (burned area),  
271 we expect that, at best, DNN-Fire would have comparable biases as BASE-Fire. Starting from  
272 DNN-Fire, we further calibrated the model weighting parameters using observed burned area  
273 from GFEDv4 between years 2001 and 2010 to create DNN-Fire-GFED. We note that the  
274 conventional approach to calibrate a process-based wildfire model requires many ensemble  
275 simulations requiring large computational resources and time. Since DNN-Fire was guided by  
276 BASE-Fire, we found that parameterization time could be substantially reduced (several minutes  
277 for the global calculation).

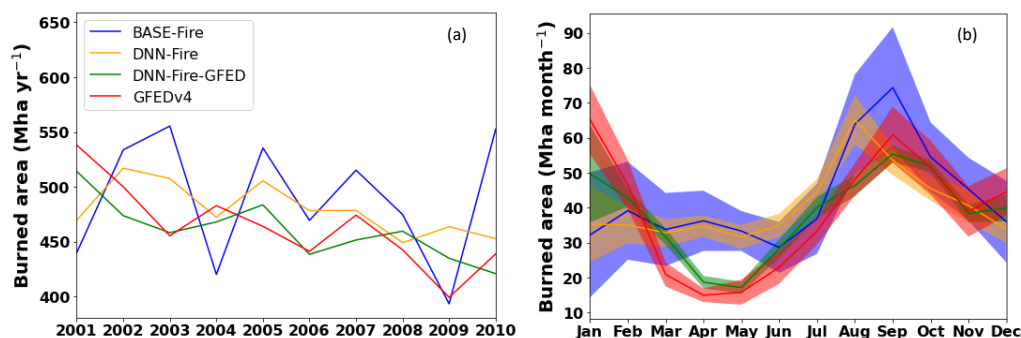
278 Dramatic improvements were found in most of the 14 GFEDv4 regions simulated by  
279 DNN-Fire-GFED (Figure 6). Overall, DNN-Fire-GFED increased simulated burned area  
280 compared to DNN-Fire by 26 Mha yr<sup>-1</sup> (73% in terms of mean absolute error averaged across all  
281 GFEDv4 regions). Pearson correlation coefficient between the DNN-Fire-GFED simulated and  
282 GFEDv4 burned area was 0.98 (*p* value < 0.001) with an *R*<sup>2</sup> of 0.97. Bias reduction was  
283 disproportionally distributed across the GFEDv4 regions (Figure 6). For example, severely  
284 burned regions, including Southern and Northern Hemisphere Africa (SHAF and NHAF) and



285 Southern Hemisphere South America (SHSA) greatly benefited from the tuning and their  
286 regional biases were reduced by 94, 64, and 44 Mha yr<sup>-1</sup> (or 90%, 83%, 95% reduction),  
287 respectively. Although Temperate Northern America (TENA) and Europe (EURO) wildfire  
288 burned area is relatively small (1-3 Mha yr<sup>-1</sup>), the impacts of wildfire activity were significant  
289 due to their high population densities. DNN-Fire tended to overestimate the burned area in  
290 TENA and EURO by 42 and 14 Mha yr<sup>-1</sup>, while DNN-Fire-GFED significantly reduced biases in  
291 both regions to less than 1 Mha yr<sup>-1</sup> (a 98% reduction).

292 BASE-Fire tended to overestimate inter-annual variability (IAV) and had opposite burned  
293 area anomalies between years 2001 and 2005. DNN-Fire dampened BASE-Fire's IAV, but had  
294 systematic overestimation of burned area. DNN-Fire-GFED agreed well with the GFEDv4  
295 observed IAV between years 2001 and 2010 (Figure 7). The seasonal cycle was also improved in  
296 DNN-Fire-GFED in terms of reducing BASE-Fire's overestimation of burned area during peak  
297 fire seasons (Figure 7), although we note that DNN-Fire-GFED is biased high during low fire  
298 seasons (March and April).

299



300

301 **Figure 7.** Inter-annual variation of burned area from years 2001 to 2010 (a) and the averaged  
302 seasonal cycle (b) of burned area estimated by the ELMv1 process-based wildfire model (BASE-  
303 Fire), Deep Neural Network wildfire model (DNN-Fire), Deep Neural Network wildfire model  
304 fine-tuned with GFEDv4 (DNN-Fire-GFED), and GFEDv4 observations.

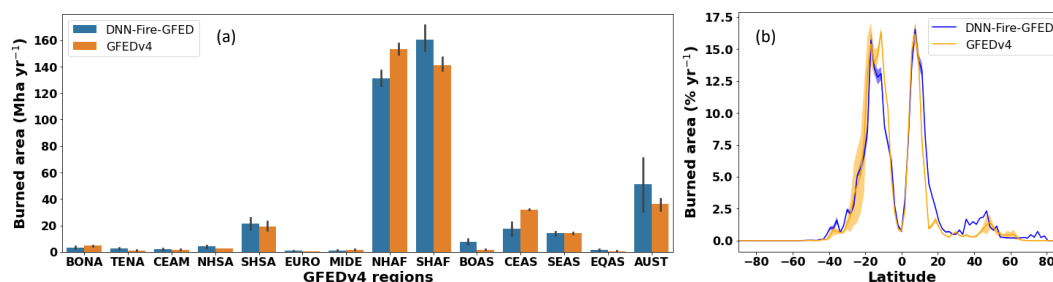
305

### 306 3.3 Prognostic simulation and limitations

307 We next evaluated the DNN-Fire-GFED model against GFEDv4 for the period 2011 to  
308 2015, using data which were not used to train and validate the model. Averaged latitudinal  
309 distribution of simulated burned area during this period showed that global wildfire activity



310 peaked around S10°- S15° and N5°-N10°, together accounting for burning 12-16% of the land  
311 surface (Figure 8). These two peaks were dominated by large burned area over Southern (SHAF)  
312 and Northern Hemisphere Africa (NHAF) fire regions. Over this period, GFEDv4 IAV was  
313 relatively larger over the Southern Hemisphere than that over the Northern Hemisphere (Figure 8  
314 shaded area). Compared to GFEDv4, DNN-Fire-GFED simulated reasonable burned area IAV  
315 over the Northern Hemisphere but lower IAV over the Southern Hemisphere. Overall, DNN-  
316 Fire-GFED simulated  $411 \pm 14$  Mha yr<sup>-1</sup> global burned area, compared with GFEDv4 observed  
317  $419 \pm 40$  Mha yr<sup>-1</sup>. DNN-Fire-GFED overestimated NHAF and Central Asia (CEAS) annual  
318 burned area by 22 and 15 Mha yr<sup>-1</sup>, respectively, while it underestimated the SHAF and Australia  
319 and New Zealand (AUST) annual burned area by 20 and 15 Mha yr<sup>-1</sup> (Figure 8, left panel). In  
320 summary, the prognostic DNN-Fire-GFED simulation is reasonably accurate and: (1) improved  
321 the simulated wildfire spatial and temporal distributions in ELMv1; (2) enabled effective and  
322 efficient parameterization of global fire.  
323



324  
325 **Figure 8.** Prognostic simulation of annual wildfire burned area with the Deep Neural Network  
326 wildfire model fine-tuned with GFEDv4 (DNN-Fire-GFED) compared with GFEDv4  
327 observations averaged over 2011-2015 for (a) 14 GFEDv4 regions and (b) latitudinal  
328 distribution.

329  
330 We acknowledge several challenges and limitations in our modeling framework. First,  
331 the original ELMv1 wildfire model has a unified mathematical representation of how fuel,  
332 climate, and social-economic conditions control wildfire burned area [Li *et al.*, 2012]. However,  
333 training one single DNN wildfire model across the globe will produce a model dominated by  
334 gridcells that have high burned area (*e.g.*, Africa). The performance of the trained DNN model,  
335 therefore, will likely have larger biases over the low fire gridcells although the globally



336 aggregated burned area could be reasonable. We partly overcame this challenge by applying the  
337 widely used 14 GFEDv4 fire regions that assume unique and relatively uniform dynamics over  
338 each region [Giglio *et al.*, 2006b]. Although the regionally specific wildfire model introduces  
339 additional complexity, it better represents distinct characteristics of wildfire activity over  
340 different climate regimes and biomes [Zhu and Zhuang, 2013; Zou *et al.*, 2019] and allows for  
341 future analyses of how the relevant controllers vary across the globe.

342

#### 343 **4. Conclusions**

344 In this study, we first surrogated the baseline ELMv1 wildfire model with a Deep Neural  
345 Network (DNN) approach (Pearson correlation coefficient = 0.91 ( $p$  value < 0.01),  $R^2 = 0.79$ ).  
346 The development was based on inputs and outputs from the baseline ELMv1 wildfire simulation,  
347 which is process-based and reasonably simulates global burned area, although regional biases  
348 existed. We then calibrated the neural network weights using the years 2001-2010 GFEDv4  
349 observationally inferred burned area. The final calibrated DNN wildfire model (DNN-Fire-  
350 GFED) was shown to be very accurate over the 14 GFED regions. For example, reductions in  
351 absolute error over Africa, South America, and Europe were over 90%. More importantly, the  
352 DNN-Fire-GFED model global parameters could be calibrated within minutes, compared with  
353 traditional ELMv1 parameterization ensemble simulations that consume a large amount of  
354 computational time. The improved DNN-Fire-GFED model also accurately prognosed global  
355 and regional burned area in the five-year period following the training period from 2011 to 2015  
356 (modeled  $411 \pm 14$  versus observed  $419 \pm 40$  Mha yr<sup>-1</sup>). We conclude that the improved surrogate  
357 wildfire model (DNN-Fire-GFED) developed in this study can serve as an effective alternative to  
358 the process-based fire model currently used in ELMv1. More broadly, we conclude that machine  
359 learning techniques can facilitate earth system model development, parameterization, and  
360 uncertainty reduction with high efficiency and accuracy.

361

#### 362 **Acknowledgements**

363 This research was supported by Energy Exascale Earth System Modeling (E3SM,  
364 <https://e3sm.org/>) Project and the Reducing Uncertainties in Biogeochemical Interactions  
365 through Synthesis and Computation (RUBISCO) Scientific Focus Area, Office of Biological and  
366 Environmental Research of the U.S. Department of Energy Office of Science. Lawrence



367 Berkeley National Laboratory (LBNL) is managed by the University of California for the U.S.  
368 Department of Energy under contract DE-AC02-05CH11231.

369

#### 370 **Author contribution**

371 Q.Z., W.J.R, designed the study, Q.Z., W.J.R, L.X., and J.T.R designed model experiments,  
372 Q.Z. and F.L. wrote code and run experiments, L.Z, K.Y, H.W., J.G all contribute to the results  
373 interpretation, and writing.

374

#### 375 **Code availability**

376 [https://github.com/qzhu-lbl/ANN\\_wildfire](https://github.com/qzhu-lbl/ANN_wildfire)

377

#### 378 **Data availability**

379 GFEDv4: [https://daac.ornl.gov/VEGETATION/guides/fire\\_emissions\\_v4.html](https://daac.ornl.gov/VEGETATION/guides/fire_emissions_v4.html)

380

#### 381 **Reference**

- 382 Abatzoglou, J. T., and A. P. Williams (2016), Impact of anthropogenic climate change on wildfire  
383 across western US forests, *Proceedings of the National Academy of Sciences*, 113(42),  
384 11770-11775.
- 385 Andela, N., D. Morton, L. Giglio, Y. Chen, G. Van Der Werf, P. Kasibhatla, R. DeFries, G. Collatz, S.  
386 Hantson, and S. Kloster (2017), A human-driven decline in global burned area, *Science*,  
387 356(6345), 1356-1362.
- 388 Arora, V. K., and G. J. Boer (2005), Fire as an interactive component of dynamic vegetation  
389 models, *Journal of Geophysical Research: Biogeosciences*, 110(G2).
- 390 Bond, W. J., F. I. Woodward, and G. F. Midgley (2005), The global distribution of ecosystems in a  
391 world without fire, *New phytologist*, 165(2), 525-538.
- 392 Bond-Lamberty, B., S. D. Peckham, D. E. Ahl, and S. T. Gower (2007), Fire as the dominant driver  
393 of central Canadian boreal forest carbon balance, *Nature*, 450(7166), 89-92.
- 394 Bowd, E. J., S. C. Banks, C. L. Strong, and D. B. Lindenmayer (2019), Long-term impacts of  
395 wildfire and logging on forest soils, *Nature Geoscience*, 12(2), 113-118.
- 396 Brando, P., B. Soares-Filho, L. Rodrigues, A. Assunção, D. Morton, D. Tuchsneider, E.  
397 Fernandes, M. Macedo, U. Oliveira, and M. Coe (2020), The gathering firestorm in  
398 southern Amazonia, *Science advances*, 6(2), eaay1632.
- 399 Cecil, D. J., D. E. Buechler, and R. J. Blakeslee (2014), Gridded lightning climatology from TRMM-  
400 LIS and OTD: Dataset description, *Atmospheric Research*, 135, 404-414.
- 401 Chambers, S., and F. Chapin (2002), Fire effects on surface-atmosphere energy exchange in  
402 Alaskan black spruce ecosystems: Implications for feedbacks to regional climate, *Journal*  
403 *of Geophysical Research: Atmospheres*, 107(D1), FFR 1-1-FFR 1-17.



- 404 Chen, Y., J. T. Randerson, S. R. Coffield, E. Foufoula-Georgiou, P. Smyth, C. A. Graff, D. C.  
405 Morton, N. Andela, G. R. van der Werf, and L. Giglio (2020), Forecasting global fire  
406 emissions on subseasonal to seasonal (S2S) time scales, *Journal of advances in modeling*  
407 *earth systems*, 12(9), e2019MS001955.
- 408 Chen, Y., J. T. Randerson, D. C. Morton, R. S. DeFries, G. J. Collatz, P. S. Kasibhatla, L. Giglio, Y.  
409 Jin, and M. E. Marlier (2011), Forecasting fire season severity in South America using sea  
410 surface temperature anomalies, *Science*, 334(6057), 787-791.
- 411 Clark, T. L., J. Coen, and D. Latham (2004), Description of a coupled atmosphere–fire model,  
412 *International Journal of Wildland Fire*, 13(1), 49-63.
- 413 Coffield, S. R., C. A. Graff, Y. Chen, P. Smyth, E. Foufoula-Georgiou, and J. T. Randerson (2019),  
414 Machine learning to predict final fire size at the time of ignition, *International journal of*  
415 *wildland fire*.
- 416 Day, C. (2004), Smoke from burning vegetation changes the coverage and behavior of clouds,  
417 *PhT*, 57(5), 24-24.
- 418 Dirmeyer, P. A., X. Gao, M. Zhao, Z. Guo, T. Oki, and N. Hanasaki (2006), GSWP-2: Multimodel  
419 analysis and implications for our perception of the land surface, *Bulletin of the American*  
420 *Meteorological Society*, 87(10), 1381-1398.
- 421 Dobson, J. E., E. A. Bright, P. R. Coleman, R. C. Durfee, and B. A. Worley (2000), LandScan: a  
422 global population database for estimating populations at risk, *Photogrammetric*  
423 *engineering and remote sensing*, 66(7), 849-857.
- 424 Finney, M. A. (1998), *FARSITE, Fire Area Simulator--model development and evaluation*, US  
425 Department of Agriculture, Forest Service, Rocky Mountain Research Station.
- 426 French, N. H., M. A. Whitley, and L. K. Jenkins (2016), Fire disturbance effects on land surface  
427 albedo in Alaskan tundra, *Journal of Geophysical Research: Biogeosciences*, 121(3), 841-  
428 854.
- 429 Ganapathi Subramanian, S., and M. Crowley (2018), Using spatial reinforcement learning to  
430 build forest wildfire dynamics models from satellite images, *Frontiers in ICT*, 5, 6.
- 431 Giglio, L., I. Csizsar, and C. O. Justice (2006a), Global distribution and seasonality of active fires  
432 as observed with the Terra and Aqua Moderate Resolution Imaging Spectroradiometer  
433 (MODIS) sensors, *Journal of geophysical research: Biogeosciences*, 111(G2).
- 434 Giglio, L., J. T. Randerson, and G. R. Van Der Werf (2013), Analysis of daily, monthly, and annual  
435 burned area using the fourth-generation global fire emissions database (GFED4),  
436 *Journal of Geophysical Research: Biogeosciences*, 118(1), 317-328.
- 437 Giglio, L., G. Van der Werf, J. Randerson, G. Collatz, and P. Kasibhatla (2006b), Global estimation  
438 of burned area using MODIS active fire observations.
- 439 Girardin, M. P., and M. Mudelsee (2008), Past and future changes in Canadian boreal wildfire  
440 activity, *Ecological Applications*, 18(2), 391-406.
- 441 Goodfellow, I., Y. Bengio, and A. Courville (2016), *Deep learning*, MIT press Cambridge.
- 442 Goss, M., D. L. Swain, J. T. Abatzoglou, A. Sarhadi, C. A. Kolden, A. P. Williams, and N. S.  
443 Diffenbaugh (2020), Climate change is increasing the likelihood of extreme autumn  
444 wildfire conditions across California, *Environmental Research Letters*, 15(9), 094016.
- 445 Harden, J. W., K. L. Manies, M. R. Turetsky, and J. C. Neff (2006), Effects of wildfire and  
446 permafrost on soil organic matter and soil climate in interior Alaska, *Global Change*  
447 *Biology*, 12(12), 2391-2403.



- 448 Heyerdahl, E. K., L. B. Brubaker, and J. K. Agee (2002), Annual and decadal climate forcing of  
449 historical fire regimes in the interior Pacific Northwest, USA, *The Holocene*, 12(5), 597-  
450 604.
- 451 Holden, Z. A., A. Swanson, C. H. Luce, W. M. Jolly, M. Maneta, J. W. Oyler, D. A. Warren, R.  
452 Parsons, and D. Affleck (2018), Decreasing fire season precipitation increased recent  
453 western US forest wildfire activity, *Proceedings of the National Academy of Sciences*,  
454 115(36), E8349-E8357.
- 455 Hurtt, G. C., L. Chini, R. Sahajpal, S. Frolking, B. L. Boudris, K. Calvin, J. C. Doelman, J. Fisk, S.  
456 Fujimori, and K. K. Goldewijk (2020), Harmonization of global land-use change and  
457 management for the period 850–2100 (LUH2) for CMIP6, *Geoscientific Model*  
458 *Development Discussions*, 1-65.
- 459 Jiang, Y., X.-Q. Yang, X. Liu, Y. Qian, K. Zhang, M. Wang, F. Li, Y. Wang, and Z. Lu (2020), Impacts  
460 of wildfire aerosols on global energy budget and climate: The role of climate feedbacks,  
461 *Journal of Climate*, 33(8), 3351-3366.
- 462 Kasischke, E. S., and L. P. Bruhwiler (2002), Emissions of carbon dioxide, carbon monoxide, and  
463 methane from boreal forest fires in 1998, *Journal of Geophysical Research:*  
464 *Atmospheres*, 107(D1), FFR 2-1-FFR 2-14.
- 465 Keeley, J. E., and A. D. Syphard (2018), Historical patterns of wildfire ignition sources in  
466 California ecosystems, *International journal of wildland fire*, 27(12), 781-799.
- 467 Kelley, D. I., I. Bistinas, R. Whitley, C. Burton, T. R. Marthews, and N. Dong (2019), How  
468 contemporary bioclimatic and human controls change global fire regimes, *Nature*  
469 *Climate Change*, 9(9), 690-696.
- 470 Kingma, D. P., and J. Ba (2014), Adam: A method for stochastic optimization, *arXiv preprint*  
471 *arXiv:1412.6980*.
- 472 Knorr, W., T. Kaminski, A. Arneth, and U. Weber (2014), Impact of human population density on  
473 fire frequency at the global scale, *Biogeosciences*, 11(4), 1085-1102.
- 474 Koven, C. D., W. J. Riley, Z. M. Subin, J. Y. Tang, M. S. Torn, W. D. Collins, G. B. Bonan, D. M.  
475 Lawrence, and S. C. Swenson (2013), The effect of vertically resolved soil  
476 biogeochemistry and alternate soil C and N models on C dynamics of CLM4,  
477 *Biogeosciences*, 10, 7109-7131.
- 478 Lamarque, J. F., J. T. Kiehl, G. P. Brasseur, T. Butler, P. Cameron-Smith, W. D. Collins, W. J.  
479 Collins, C. Granier, D. Hauglustaine, and P. G. Hess (2005), Assessing future nitrogen  
480 deposition and carbon cycle feedback using a multimodel approach: Analysis of nitrogen  
481 deposition, *Journal of Geophysical Research: Atmospheres*, 110(D19).
- 482 Lenihan, J. M., and D. Bachelet (2015), Historical climate and suppression effects on simulated  
483 fire and carbon dynamics in the conterminous United States, *Global Vegetation*  
484 *Dynamics: Concepts and Applications in the MC1 Model*, edited by: Bachelet, D. and  
485 Turner, D., *AGU Geophysical Monographs*, 214, 17-30.
- 486 Li, F., M. Val Martin, M. O. Andreae, A. Arneth, S. Hantson, J. W. Kaiser, G. Lasslop, C. Yue, D.  
487 Bachelet, and M. Forrest (2019), Historical (1700–2012) global multi-model estimates of  
488 the fire emissions from the Fire Modeling Intercomparison Project (FireMIP),  
489 *Atmospheric Chemistry and Physics*, 19(19), 12545-12567.
- 490 Li, F., X. Zeng, and S. Levis (2012), A process-based fire parameterization of intermediate  
491 complexity in a Dynamic Global Vegetation Model, *Biogeosciences*, 9(7).



- 492 Mahowald, N., T. D. Jickells, A. R. Baker, P. Artaxo, C. R. Benitez-Nelson, G. Bergametti, T. C.  
493 Bond, Y. Chen, D. D. Cohen, and B. Herut (2008), Global distribution of atmospheric  
494 phosphorus sources, concentrations and deposition rates, and anthropogenic impacts,  
495 *Global Biogeochemical Cycles*, 22(4).
- 496 Mekonnen, Z. A., W. J. Riley, J. T. Randerson, R. F. Grant, and B. M. Rogers (2019), Expansion of  
497 high-latitude deciduous forests driven by interactions between climate warming and  
498 fire, *Nature plants*, 5(9), 952-958.
- 499 Oliver, A. K., M. A. Callahan Jr, and A. Jumpponen (2015), Soil fungal communities respond  
500 compositionally to recurring frequent prescribed burning in a managed southeastern US  
501 forest ecosystem, *Forest Ecology and Management*, 345, 1-9.
- 502 Papakosta, P., G. Xanthopoulos, and D. Straub (2017), Probabilistic prediction of wildfire  
503 economic losses to housing in Cyprus using Bayesian network analysis, *International  
504 journal of wildland fire*, 26(1), 10-23.
- 505 Pellegrini, A. F., A. Ahlström, S. E. Hobbie, P. B. Reich, L. P. Nieradzik, A. C. Staver, B. C.  
506 Scharenbroch, A. Jumpponen, W. R. Anderegg, and J. T. Randerson (2018), Fire  
507 frequency drives decadal changes in soil carbon and nitrogen and ecosystem  
508 productivity, *Nature*, 553(7687), 194-198.
- 509 Pellegrini, A. F., S. E. Hobbie, P. B. Reich, A. Jumpponen, E. J. Brookshire, A. C. Caprio, C.  
510 Coetsee, and R. B. Jackson (2020), Repeated fire shifts carbon and nitrogen cycling by  
511 changing plant inputs and soil decomposition across ecosystems, *Ecological  
512 Monographs*, e01409.
- 513 Preisler, H. K., and A. L. Westerling (2007), Statistical model for forecasting monthly large  
514 wildfire events in western United States, *Journal of Applied Meteorology and  
515 Climatology*, 46(7), 1020-1030.
- 516 Prentice, S., and D. Mackerras (1977), The ratio of cloud to cloud-ground lightning flashes in  
517 thunderstorms, *Journal of Applied Meteorology*, 16(5), 545-550.
- 518 Radke, D., A. Hessler, and D. Ellsworth (2019), FireCast: Leveraging Deep Learning to Predict  
519 Wildfire Spread, paper presented at IJCAI.
- 520 Randerson, J. T., H. Liu, M. G. Flanner, S. D. Chambers, Y. Jin, P. G. Hess, G. Pfister, M. Mack, K.  
521 Treseder, and L. Welp (2006), The impact of boreal forest fire on climate warming,  
522 *science*, 314(5802), 1130-1132.
- 523 Riley, K., and M. Thompson (2017), An uncertainty analysis of wildfire modeling, *Natural hazard  
524 uncertainty assessment: modeling and decision support. Monograph*, 223, 193-213.
- 525 Ross, A. N., M. J. Wooster, H. Boesch, and R. Parker (2013), First satellite measurements of  
526 carbon dioxide and methane emission ratios in wildfire plumes, *Geophysical Research  
527 Letters*, 40(15), 4098-4102.
- 528 Rother, D., and F. De Sales (2020), Impact of Wildfire on the Surface Energy Balance in Six  
529 California Case Studies, *Boundary-Layer Meteorology*, 1-24.
- 530 Saha, M. V., T. M. Scanlon, and P. D'Odorico (2019), Climate seasonality as an essential  
531 predictor of global fire activity, *Global Ecology and Biogeography*, 28(2), 198-210.
- 532 Sayad, Y. O., H. Mousannif, and H. Al Moatassime (2019), Predictive modeling of wildfires: A  
533 new dataset and machine learning approach, *Fire safety journal*, 104, 130-146.
- 534 Schmidhuber, J. (2015), Deep learning in neural networks: An overview, *Neural networks*, 61,  
535 85-117.



- 536 Stephenson, C., J. Handmer, and R. Betts (2013), Estimating the economic, social and  
537 environmental impacts of wildfires in Australia, *Environmental Hazards*, 12(2), 93-111.
- 538 Syphard, A. D., V. C. Radeloff, J. E. Keeley, T. J. Hawbaker, M. K. Clayton, S. I. Stewart, and R. B.  
539 Hammer (2007), Human influence on California fire regimes, *Ecological applications*,  
540 17(5), 1388-1402.
- 541 Teckentrup, L., G. Lasslop, D. Bachelet, M. Forrest, S. Hantson, F. Li, J. R. Melton, C. Yue, A.  
542 Arneeth, and S. P. Harrison (2018), Simulations of historical burned area: A comparison of  
543 global fire models in FireMIP, *EGUGA*, 17537.
- 544 Thonicke, K., A. Spessa, I. Prentice, S. P. Harrison, L. Dong, and C. Carmona-Moreno (2010), The  
545 influence of vegetation, fire spread and fire behaviour on biomass burning and trace gas  
546 emissions: results from a process-based model, *Biogeosciences*, 7(6), 1991-2011.
- 547 Tonini, M., M. D'Andrea, G. Biondi, S. Degli Esposti, A. Trucchia, and P. Fiorucci (2020), A  
548 Machine Learning-Based Approach for Wildfire Susceptibility Mapping. The Case Study  
549 of the Liguria Region in Italy, *Geosciences*, 10(3), 105.
- 550 van Vuuren, D. P., P. L. Lucas, and H. Hilderink (2007), Downscaling drivers of global  
551 environmental change: Enabling use of global SRES scenarios at the national and grid  
552 levels, *Global environmental change*, 17(1), 114-130.
- 553 Venevsky, S., K. Thonicke, S. Sitch, and W. Cramer (2002), Simulating fire regimes in human-  
554 dominated ecosystems: Iberian Peninsula case study, *Global Change Biology*, 8(10), 984-  
555 998.
- 556 Walker, X. J., J. L. Baltzer, S. G. Cumming, N. J. Day, C. Ebert, S. Goetz, J. F. Johnstone, S. Potter,  
557 B. M. Rogers, and E. A. Schuur (2019), Increasing wildfires threaten historic carbon sink  
558 of boreal forest soils, *Nature*, 572(7770), 520-523.
- 559 Westerling, A. L., H. G. Hidalgo, D. R. Cayan, and T. W. Swetnam (2006), Warming and earlier  
560 spring increase western US forest wildfire activity, *science*, 313(5789), 940-943.
- 561 Williams, A. P., J. T. Abatzoglou, A. Gershunov, J. Guzman-Morales, D. A. Bishop, J. K. Balch, and  
562 D. P. Lettenmaier (2019), Observed impacts of anthropogenic climate change on wildfire  
563 in California, *Earth's Future*, 7(8), 892-910.
- 564 Xu, X., G. Jia, X. Zhang, W. J. Riley, and Y. Xue (2020), Climate regime shift and forest loss  
565 amplify fire in Amazonian forests, *Global Change Biology*, 26(10), 5874-5885.
- 566 Yu, Y., J. Mao, P. E. Thornton, M. Notaro, S. D. Wullschleger, X. Shi, F. M. Hoffman, and Y. Wang  
567 (2020), Quantifying the drivers and predictability of seasonal changes in African fire,  
568 *Nature Communications*, 11(1), 1-8.
- 569 Yue, X., L. J. Mickley, J. A. Logan, and J. O. Kaplan (2013), Ensemble projections of wildfire  
570 activity and carbonaceous aerosol concentrations over the western United States in the  
571 mid-21st century, *Atmospheric Environment*, 77, 767-780.
- 572 Zheng, H., Z. Yang, W. Liu, J. Liang, and Y. Li (2015), Improving deep neural networks using  
573 softplus units, paper presented at 2015 International Joint Conference on Neural  
574 Networks (IJCNN), IEEE.
- 575 Zhu, Q., and W. J. Riley (2015), Improved modelling of soil nitrogen losses, *Nature Climate  
576 Change*, 5(8), 705-706.
- 577 Zhu, Q., W. J. Riley, C. M. Iversen, and J. Kattge (2020), Assessing impacts of plant stoichiometric  
578 traits on terrestrial ecosystem carbon accumulation using the E3SM land model, *Journal  
579 of Advances in Modeling Earth Systems*, 12(4), e2019MS001841.



- 580 Zhu, Q., W. J. Riley, J. Tang, N. Collier, F. M. Hoffman, X. Yang, and G. Bisht (2019), Representing  
581 nitrogen, phosphorus, and carbon interactions in the E3SM Land Model: Development  
582 and global benchmarking, *Journal of Advances in Modeling Earth Systems*, doi:  
583 10.1029/2018MS001571.
- 584 Zhu, Q., W. J. Riley, J. Tang, and C. D. Koven (2016), Multiple soil nutrient competition between  
585 plants, microbes, and mineral surfaces: model development, parameterization, and  
586 example applications in several tropical forests, *Biogeosciences*, *13*, 341-363,  
587 doi:10.5194/bgd-12-4057-2015.
- 588 Zhu, Q., and Q. Zhuang (2013), Improving the quantification of terrestrial ecosystem carbon  
589 dynamics over the United States using an adjoint method, *Ecosphere*, *4*(10), doi:  
590 dx.doi.org/10.1890/ES1813-00058.00051.
- 591 Zhu, Q., and Q. Zhuang (2014), Parameterization and sensitivity analysis of a process-based  
592 terrestrial ecosystem model using adjoint method, *Journal of Advances in Modeling  
593 Earth Systems*, *6*(2), 315-331.
- 594 Zou, Y., Y. Wang, Z. Ke, H. Tian, J. Yang, and Y. Liu (2019), Development of a REgion-specific  
595 ecosystem feedback fire (RESFire) model in the Community Earth System Model, *Journal  
596 of Advances in Modeling Earth Systems*, *11*(2), 417-445.
- 597 Zou, Y., Y. Wang, Y. Qian, H. Tian, J. Yang, and E. Alvarado (2020), Using CESM-RESFire to  
598 understand climate-fire-ecosystem interactions and the implications for decadal climate  
599 variability, *Atmospheric Chemistry and Physics*, *20*(PNNL-SA-150222).
- 600